

# **THERMAL MODELING OF METAL POWDER-BASED SELECTIVE LASER SINTERING**

Tiebing Chen and Yuwen Zhang

Department of Mechanical and Aerospace Engineering, University of Missouri-Columbia,  
Columbia, MO 65211

**Reviewed, accepted August 3, 2005**

## **Abstract**

In order to get a better understanding of Selective Laser Sintering (SLS) process of the metal powders, three-dimensional modeling of laser sintering of a metal powder mixture that contains two kinds of metal powder with significantly different melting points under a moving Gaussian laser beam is investigated numerically. Laser induced melting and resolidification accompanied by shrinkage are modeled using a temperature transforming model. The liquid flow of the melted low melting point metal driven by capillary and gravity forces is also included in the physical model. Both complete and partial shrinkages are considered in the model. Simulations are performed for both single line laser scanning and multiple-line laser scanning. The numerical results are compared with experimental results and a detailed parametric study is performed. The effects of the moving heat source intensity, the scanning velocity, the thickness of the powder layer and the number of existing sintered layers underneath on the sintering depth, the shape of the heat affected zone (HAZ) and the temperature distribution are discussed. The optimized dimensionless moving heat source intensity increases with increasing scanning velocity in order to achieve the desired sintering depth and bond the newly sintered layer to the previously sintered layers.

## **Introduction**

Selective Laser Sintering (SLS) is a rapid prototyping/manufacturing technology that can build structurally-sound parts of near full density from powdered material via layer-by-layer sintering (for amorphous powder, such as polycarbonate) or melting (for crystalline powder, such as metal) induced by a directed laser beam [1]. Fabrication of metal part is very challenge task since the temperature required to bind the metal powder particles is much higher than that to bind the amorphous powders particles. During the SLS process, a thin (100 - 250 m thick) powder layer is laser-scanned to fuse the two-dimensional slice to an underlying solid piece, which consists of a series of stacked and fused two-dimensional slices. After laser scanning, a fresh powder layer is spread and the scanning process is repeated. Loose powder is removed after the part is extracted from its bin. The advantages of SLS over other gas-based SFF technologies include (a) the production rate is much higher, and (b) the over-hanging structures can be supported by the loose powders.

Direct SLS of metal powder is very complex and the specific metal powders used must be chosen carefully. One problem that encountered in the metal powder sintering process is the “balling” phenomenon, which is the formation of a series of spheres with the size approximately equal to the diameter of laser beam due to the surface tension. Another problem lies in achieving dimensional stability during the sintering process, which results from the shrinkage causing poor bonding between the scanning lines and layers. Two different metal powder systems have been developed by the researchers in order to solve the problems mentioned above. One is the single-component powder approach which overcomes the “balling” phenomenon by scanning at very

high velocities with very small beam spot sizes [2], and the other is the two-component powder approach which uses two types of the metal powders possessing significantly different melting points [3, 4]. The high melting point powder remains solid in the sintering process and plays an important role as the support structure necessary to avoid “balling”. Solidification of the low melting point metal bonds the high melting point metal powder particles together to form the part layers. The particular material properties and methods of material analysis of the metal-based powder system for SLS applications are addressed by Storch et al. [5]. Effects of laser sintering processing parameters on the microstructure and densification of iron powder was investigated by Simchi and Pohl [6]. A case study on the development of direct metal laser sintering for rapid tooling was performed by Simchi et al. [7]. A thorough examination on direct SLS in addition to fundamental issues on SFF is addressed by Lu et al. [8]. Experimental studies of direct SLS have received many attentions [9-12]. Modeling approaches have been addressed more and more recently [13-14].

A one-dimensional thermal model of melting of the two-component metal powder bed was presented by Mughal and Plumb [15], where a constant porosity model was developed and the liquid motion caused by capillary and gravity forces was considered but the shrinkage was neglected. Zhang and Faghri [16] analytically solved a one-dimensional melting problem in a semi-infinite powder bed containing a mixture of the powder subjected to a constant heat flux heating. Effects of the porosity of the solid phase, initial subcooling parameter and dimensionless thermal conductivity of gas were investigated. A two-dimensional steady-state laser-melting problem using an Alternative Direction Implicit (ADI) scheme with a false transient formulation was solved by Basu and Srinivasan [17]. A numerical simulation of the two-dimensional melting and resolidification of subcooled semi-infinite metal powder bed with a moving Gaussian heat source was presented by Zhang and Faghri [18]. Raman and German [19] investigated liquid-phase sintering consisting of interconnected crystalline grains in a homogeneous matrix phase and gave a mathematical model for gravity-induced distortion in order to achieve the dimensional stability. Kou and Wang [20] investigated three-dimensional convection in laser melted pools and the effect of surface tension temperature coefficient on the convection pattern and penetration of laser melted pools was demonstrated. A three-dimensional finite element simulation for temperature evolution in the SLS process was demonstrated by Kolossov et al. [21], where the non-linear behavior of thermal conductivity and of specific heat due to temperature changes and phase transformations were considered. A three-dimensional thermal model of SLS of two-component metal powder bed was presented by Zhang et al. [22], where the solid particle velocity induced by shrinkage of the powder bed and a liquid flow driven by capillary and gravity forces were taken into account.

The thickness of the computational domain perpendicular to the direction of the moving laser beam used in Ref. [22] was very large, which approximated SLS of the first layer of the metal powders. In the present paper, the sintering processes in a three-dimensional finite metal powder layer with adiabatic bottom or on top of multiple sintered layers are investigated. A partial shrinkage model of SLS of two-component metal powder is developed and the effects of partial shrinkage on the SLS process are addressed. In order to obtain the sound metallic bonding between sintered layers, the overlaps not only between vertically deposited layers but also layers at horizontal neighbors are considered. The effects of the porosity in HAZ, laser intensity, and laser scanning velocity speed the shape of the HAZ are investigated

### Physical Models and Problem Statement

Three different physical models of melting and resolidification in SLS process as shown in Fig. 1 will be studied in this paper. Fig. 1 (a) shows melting and resolidification in a powder layer with adiabatic bottom surface. A circular Gaussian laser beam moves at a constant velocity,  $u_b$ , over the surface of a two-component metal powder layer. A moving coordinate system of which the origin is fixed at the center of heat source is employed. The initial temperature of the powder layer is below the melting point of the low melting point powder,  $T_m$ . As the laser beam interacts with the powders, the temperature of the powders is brought up to  $T_m$  then melting occurs. A liquid pool is formed under the laser beam and the molten metal infiltrates the unsintered powders driven by capillary and gravitational forces. A densified heat affected zone (HAZ) is formed after the laser beam moves away and the liquid pool resolidifies. The significant density change due to the shrinkage accompanying with melting is also taken into account. Figure 1(b) shows melting and resolidification of a loose powder layer on top of the multiple previously sintered layers. A single line scanning of the laser beam is considered, therefore, half of the physical domain is considered because of the symmetry. The overlap between the newly sintered layer and pre-deposited sintered layers underneath in order to obtain the sound metallic bonding is considered. The overlap between layers is defined as the ratio of the width of the liquid pool at the bottom surface of the fresh layer to that of the liquid pool at the top surface. Figure 1(c) shows the sintering process with the multiple-line scanning in a loose powder layer with multiple previously sintered layers underneath. During the SLS process, the position of the laser beam will be reset and begin to start another scanning line along X direction. The scan spacing determines the amount of overlap between adjacent lines. The value of overlap between lines is assumed to be 0.5 in this paper in order to get optimum bonding which aids densification. After the completion of the sintering process on X-Y plane, the sintered layer is lowered and a fresh layer of powders is allowed to be spread into the build zone in order to repeat the process. The multiple-line scanning problems can be simplified into a single laser scanning by considering half powder layer which is orthogonal to the laser scanning direction has been sintered and resolidified. The half region in negative Y direction is not the layer of fresh powders but sintered due to the overlap. The initial top surface of the physical domain before the sintering process is not a flat surface for all cases again. The configuration of previous scan line at neighbor needs to be considered. The shape of the previous sintered region can be estimated by the regression of the HAZ shape in single scan line model with the same porosity and number of existed sintered layers below. Therefore, the physical domain will have different shapes of the top surface for different porosity, i.e., rate of shrinkage.

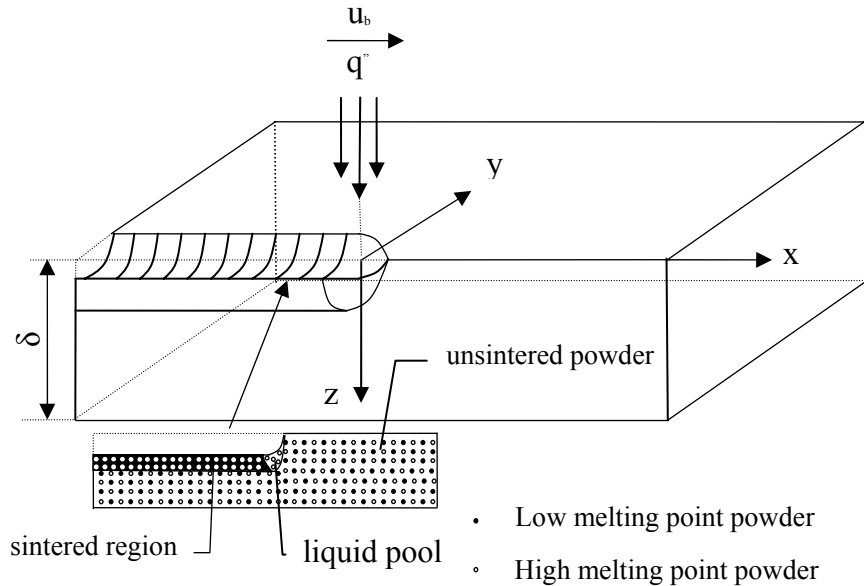
While the complete shrinkage model is assumed in the physical problem of Fig. 1(a), the partial shrinkage model is integrated into the physical problems of Figs 1(b) and (c). The loose powder bed contains high melting point powder ( $H$ ), low melting point powder ( $s$ ), and gas ( $g,s$ ; gas in loose powder). The volume fraction of all components add up to unity, i.e.,  $\varphi_H + \varphi_s + \varphi_{g,s} = 1$ . Upon melting, the liquid pool contains high melting point powder ( $H$ ), liquid ( $\ell$ ) of low melting point component, and gas ( $g,\ell$ ; gas in liquid region) and their volume fractions satisfies  $\varphi_H + \varphi_\ell + \varphi_{g,\ell} = 1$ , which is also applicable in the resolidified region if  $\varphi_\ell$  represents volume fraction of the resolidified low melting point component. The porosity,  $\varepsilon$ , defined as volume fraction of void that can be occupied by either gas or liquid, is equal to  $\varphi_{g,s}$

in the loose powder and it becomes  $\varphi_\ell + \varphi_{g,\ell}$  after melting. If the volume of the gas being driven out from the powder bed is equal to the volume of the liquid generated during melting, the porosity of the powder bed before and after melting will be the same, i.e.,  $\varepsilon = \varphi_{g,s} = \varphi_s + \varphi_{g,\ell}$ , which is referred to as constant porosity model [22,23]. If the volume fractions of high and low melting point powders before sintering satisfy  $\varphi_s / (\varphi_H + \varphi_s) = \varphi_{g,s}$ , the powder bed can be fully densified ( $\varphi_{g,\ell} = 0$ ) under constant porosity model [22, 23]. On the other hand, if there is no shrinkage, one would expect that  $\varphi_{g,\ell} = \varphi_{g,s}$  and the porosity,  $\varepsilon$ , will increase since  $\varphi_\ell$  increases during melting. The complete shrinkage under constant porosity model and no shrinkage represent two extremes in SLS of two-component metal powders. Under the partial shrinkage model to be developed, the different shrinkage rates during melting is represented by the volume fraction of gas in the liquid pool,  $\varphi_{g,\ell}$ .

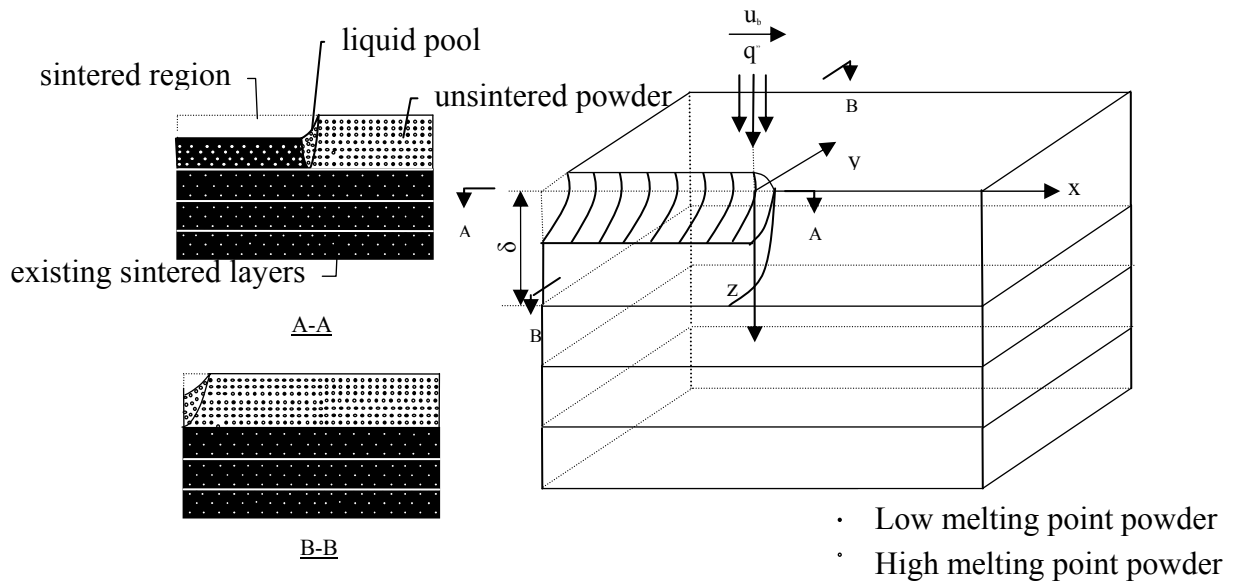
The problem is formulated using a temperature transforming model [24]. The governing equation and the corresponding boundary and initial conditions will be given in dimensionless form.

$$\begin{aligned} & \nabla \cdot (\varphi_\ell \mathbf{V}_\ell C_L T) - U_b \frac{\partial}{\partial X} [(\varphi_H + \varphi_s C_L) T] + W_s \frac{\partial}{\partial Z} [(\varphi_H + \varphi_s C_L) T] \\ & = \nabla \cdot (K \nabla T) - \left\{ \frac{\partial}{\partial \tau} [(\varphi_\ell + \varphi_s) S] + \nabla \cdot (\varphi_\ell \mathbf{V}_\ell S) + W_s \frac{\partial}{\partial Z} (\varphi_s S) - U \frac{\partial}{\partial X} [(\varphi_\ell + \varphi_s) S] \right\} \end{aligned} \quad (1)$$

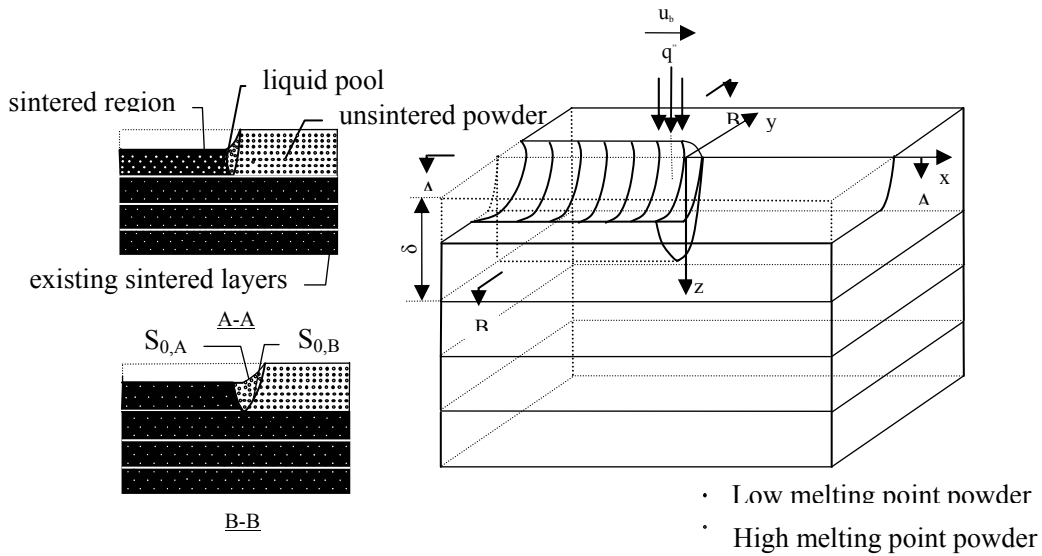
where the dimensionless shrinkage velocity,  $W_s$ , heat capacity,  $C$ , source term,  $S$ , and thermal conductivity,  $K$ , can be given by



(a) SLS of single layer



(b) Single-line scanning of loose powder on existing sintered layers



(c) Multiple line scanning of loose powder on existing sintered layers

Fig. 1 Physical Model

$$W_s = \begin{cases} \frac{\varphi_{si}}{1-\varepsilon} \left( \frac{\partial \eta_{st}}{\partial \tau} - U \frac{\partial \eta_{st}}{\partial X} \right) & Z \leq \eta_{st} \leq \Delta \\ 0 & Z > \eta_{st} \end{cases} \quad (2)$$

$$C = (\varphi_s + \varphi_l) C_L + \varphi_H \quad (3)$$

$$C_L = \begin{cases} C_L & T < -\Delta T \\ C_L \left( 1 + \frac{1}{2Sc\Delta T} \right) & -\Delta T < T < \Delta T \\ C_L & T > \Delta T \end{cases} \quad (4)$$

$$S = \begin{cases} 0 & T < -\Delta T \\ \frac{C_L}{2Sc} & -\Delta T < T < \Delta T \\ \frac{C_L}{Sc} & T > \Delta T \end{cases} \quad (5)$$

$$K = \begin{cases} K_{eff} & T < -\Delta T \\ K_{eff} + \frac{K_\ell - K_{eff}}{2\Delta T} (T + \Delta T) & -\Delta T < T < \Delta T \\ K_\ell & T > \Delta T \end{cases} \quad (6)$$

$$K_\ell = (\varphi_\ell + \varphi_s)K_L + \varphi_H \quad (7)$$

where  $K_{eff}$  is the dimensionless effective thermal conductivity of the loose powder region [18].

The dimensionless velocities of the liquid phase,  $\mathbf{V}_\ell$ , can be obtained by Darcy's law. The dimensionless equation of Darcy's law is

$$\mathbf{V}_\ell - (-U_b \mathbf{i} + W_s \mathbf{k}) = \frac{\varepsilon Ma \psi_e^3}{\sqrt{180(1-\varepsilon)^2 \psi}} \nabla P_c + \frac{\varepsilon^2 Ma Bo \psi_e^3}{180(1-\varepsilon)^2 \psi} \mathbf{k} \quad (8)$$

where the two parameters,  $Ma$  and  $Bo$ , in eq. (4-8) are defined as

$$Ma = \frac{\gamma_m^0 d_p}{\alpha_H \mu}, \quad Bo = \frac{\rho_\ell g R d_p}{\gamma_m^0} \quad (9)$$

The dimensionless capillary pressure,  $P_c$ , in eqs. (4-8) can be calculate by [25].

$$P_c = 1.417(1-\psi_e) - 2.12(1-\psi_e)^2 + 1.263(1-\psi_e)^3 \quad (10)$$

The normalized saturation,  $\psi_e$ , in eq. (4-8) is obtained by

$$\psi_e = \begin{cases} \frac{\psi - \psi_{ir}}{1 - \psi_{ir}} & \psi > \psi_{ir} \\ 0 & \psi \leq \psi_{ir} \end{cases} \quad (11)$$

where  $\psi_{i,r}$  is the irreducible saturation. Equation (8) satisfies the dimensionless continuity equation of the liquid, which is obtained by

$$\frac{\partial \varphi_\ell}{\partial \tau} + \nabla \cdot (\varphi_\ell \mathbf{V}_\ell) = \dot{\Phi}_L \quad (12)$$

The continuity equations for the solid phase of the low melting point powder and high melting point powder by assuming shrinkage occurs in the z- direction only are

$$\frac{\partial \varphi_s}{\partial \tau} - U_b \frac{\partial \varphi_s}{\partial X} + \frac{\partial (\varphi_s w_s)}{\partial Z} = -\dot{\Phi}_L \quad (13)$$

$$\frac{\partial \varphi_H}{\partial \tau} - U_b \frac{\partial \varphi_H}{\partial X} + \frac{\partial(\varphi_H W_s)}{\partial Z} = 0 \quad (14)$$

The following relationship is valid in all regions

$$\varepsilon + \varphi_s + \varphi_H = 1 \quad (15)$$

Combined with eqs. (12-15), the volume production rate,  $\dot{\Phi}_L$ , is obtained:

$$\dot{\Phi}_L = -\frac{\partial(1-\varepsilon)}{\partial \tau} + U_b \frac{\partial(1-\varepsilon)}{\partial X} - \frac{\partial}{\partial Z} [(1-\varepsilon)W_s] \quad (16)$$

The volume fraction of the solid particles of the low melting point powder is determined by

$$\varphi_s = \begin{cases} \varphi_{si} & Z > \eta_{st} \\ 0 & Z < \eta_{st} \end{cases} \quad (17)$$

The corresponding boundary and initial conditions of eq. (1) is

$$-K \frac{\partial T}{\partial Z} = N_i \exp(-X^2) - N_R [(T + N_i)^4 - (T_\infty + N_i)^4] - Bi(T - T_\infty) \quad Z = \eta_0(X) \quad (18)$$

$$\frac{\partial T}{\partial Z} = 0, \quad -\infty < X < \infty, \quad 0 \leq Y < \infty, \quad Z = \Delta_s + N\Delta_p, \quad \tau > 0 \quad (19)$$

$$T = -1, \quad -\infty < X < \infty, \quad 0 \leq Y < \infty, \quad 0 < Z < \Delta_s + N\Delta_p, \quad \tau = 0 \quad (20)$$

The location of liquid surface is related to the sintered depth with the assumption that the sintered layers are fully densitized, i.e.,

$$\eta_0(X, Y) = \begin{cases} \frac{1 - \varepsilon_\ell - \varphi_{H,i}}{1 - \varepsilon_\ell} \eta_{st}(X, Y) & \eta_{st} < \Delta_s \\ \frac{1 - \varepsilon_\ell - \varphi_{H,i}}{1 - \varepsilon_\ell} \Delta_s & \eta_{st} \geq \Delta_s \end{cases} \quad (21)$$

For the complete shrinkage, the porosity,  $\varepsilon$ , is constant. Then eqs. (16) and (21) can be simplified.  $N$  is equal to 0 for the sintering process in the single powder layer.

### Numerical Solution

The sintering problem specified by the governing eq. (1) is a three-dimensional, transient and nonlinear problem. The converged steady-state solution of eq. (1) with its corresponding boundary conditions in a moving coordinate system can be obtained by a finite volume method [26]. The conduction-convection terms are interpreted by the power-law scheme. The computational domain in the physical model has an irregular shape which includes the unsintered powders, liquid pool and resolidified region due to the shrinkage. The block-off approach [26] is employed to deal with the irregular geometric shape. The thermal conductivity in the empty space created by the shrinkage is zero. The dimension in  $X$  direction is large enough compared with the order of magnitude of the diameter of the moving laser beam in order to obtain the quasi-steady-state solution. The computation was carried out using a non-uniform grid in the  $X$  and  $Y$  directions and uniform grid in the  $Z$  direction. The dimensionless time step was 0.12 and the grid number used in the numerical simulation was  $92 \times (37 \sim 72) \times (22 \sim 42)$ , depending on the width and thickness of the metal powder layer. Smaller time steps and finer grids were also used in the simulation but no noticeable difference is found. The dimensionless phase-

change temperature range,  $\Delta T$ , is chosen to be 0.001 in order to simulate melting and resolidification occurring at a single temperature.

### Results and discussions

Successful fabrication of metal parts requires a careful match between the surface properties of the two materials. The liquid phase low melting point material must wet the non-melting solid particles in order to fabricate full density parts. Identification of powder pairs with these characteristics is not trivial and hence specific materials are used here [18]. Simulations were conducted using a mixture of 40% nickel braze powder and 60% AISI 1018 carbon steel powder by volume. The initial porosity of the powder was chosen to be 0.42 based on a simple mass/volume measurement procedure by Zhang et al. [22]. The effect of the moving laser beam intensity, scanning velocity and the thickness of the powder layer, which are dominant parameters for a three-dimensional process, will be investigated numerically. The thermal properties of the AISI 1018 steel and nickel braze in the powder mixture are available in the reference [22]. The dimensionless parameters that are used in the numerical simulation are shown in Table 1.

Table 1 Sintering parameters applied in the numerical simulation

$B_i$	$2.94 \times 10^{-4}$	$N_R$	$4.2 \times 10^{-4}$
$Bo$	$5.3 \times 10^{-3}$	$Sc$	1.38
$C_L$	1.07	$T_\infty$	-1.0
$K_g$	$5.38 \times 10^{-4}$	$\varepsilon_s$	0.4
$K_L$	0.2	$\varphi_{si}$	0.24
$Ma$	1042.0	$\psi_{ir}$	0.08
$N_g$	$1.19 \times 10^{-3}$	$\Delta T$	0.001

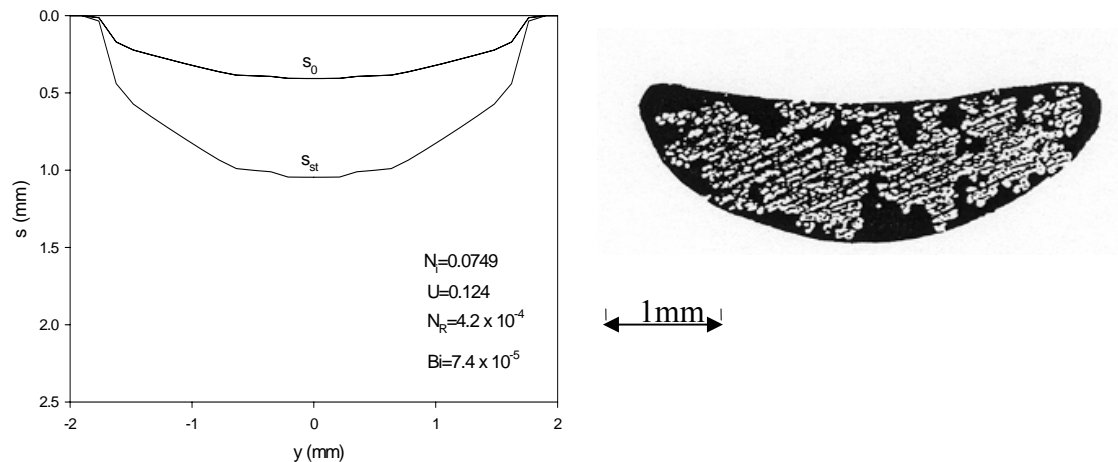


Fig. 2 Comparison of numerical and experimental solutions

In order to validate the simulation results, the comparison between the numerical and experimental results was performed. The experimental result and corresponding processing parameters were obtained from Zhang et al. [22]. The dimensionless moving laser beam intensity is 0.0749 and corresponding dimensionless scanning velocity is 0.124. The comparison of the

cross-sections obtained by numerical simulation and experiment was shown in Fig. 2. The black area in the micrograph is a local void and the light area is sintered metal. It can be seen that the actual and predicted shapes of the HAZ are similar, but large degree of local porosity exists in the experimentally observed HAZ. Thicknesses of the sintered HAZ are greatest at the center of the beam and decreases with increasing  $y$ .

### SLS of Single Powder Layer

Figure 3 shows the three-dimensional configuration of the powder layer surfaces and HAZ produced by sintering with a moving laser beam. The space above the surface  $\eta_0$  is void due to the top depression induced by the shrinkage of the powder layer. A liquid pool is generated by the moving laser beam and then resolidified after the laser beam moved away. The volume of the liquid pool is relatively small since the thickness of the powder layer is very small and then a relatively small magnitude of the laser beam intensity is applied. The three-dimensional temperature distribution on the surface of the powder layer at the quasi-steady-state during the sintering process is shown in the Fig. 4.

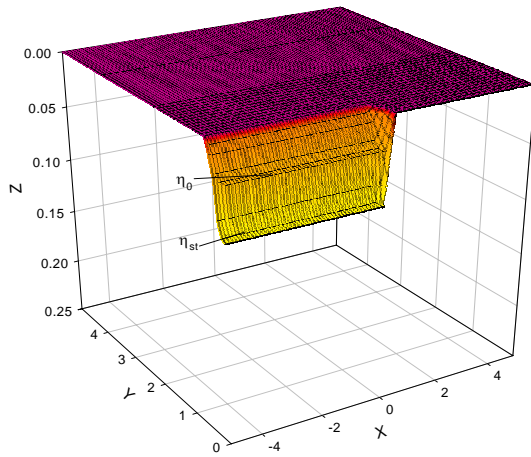


Fig. 3 Three-dimensional shape of the HAZ ( $\Delta = 0.25$ ,  $U_b = 0.1$ ,  $N_i = 0.0125$ )

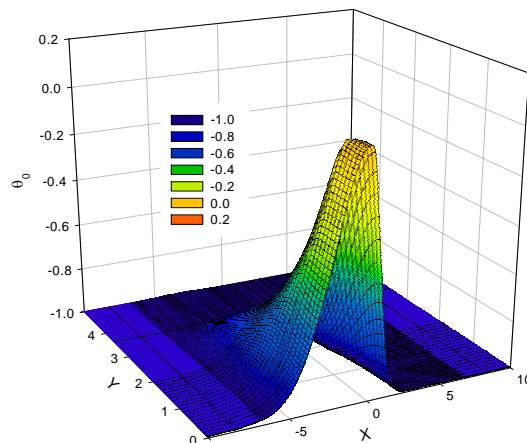


Fig. 4 The surface temperature distribution ( $\Delta = 0.25$ ,  $U_b = 0.1$ ,  $N_i = 0.0125$ )

### Single-line scanning of loose powder on existing sintered layers

The three dimensional shape of Heat Affected Zone (HAZ) sintered by a moving circular laser beam with respect to different volume fraction of the gas in the liquid pool with one existing sintered layer below for single laser scan line are shown in Figs. 5-7. The overlap between the liquid pool and existing sintered layers below are considered in order to bond the newly deposited layer with the existing sintered layers tightly. The shrinkage is smaller when the volume fraction of gas in the liquid pool increases. There is no shrinkage when the volume fractions of gas in the liquid pool and the loose powder are equal since the gas trapped in the void among the powder particles are not released. The higher moving laser beam intensity is needed for the sintering process with higher volume fraction of the gas in the liquid pool in order to obtain the same sintering depth. That is because the higher volume fraction of the gas in the liquid pool causes the smaller rate of the shrinkage and thicker existing sintered layers below.

Besides, the higher magnitude of the laser power is needed since the thermal conductivity of the existed sintered layers is much higher than that of the loose powder layer.

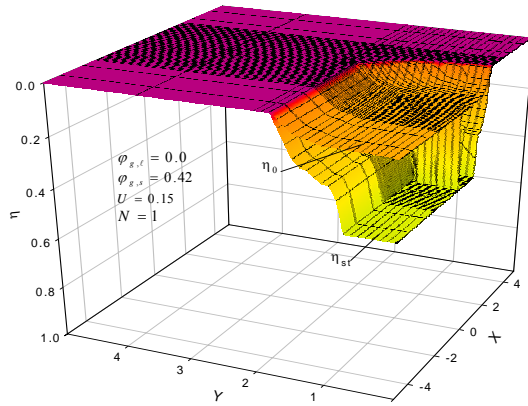


Fig. 5 Three-dimensional shape of the HAZ ( $\Delta_s = 0.25, U_b = 0.15, N = 1, \varphi_{g,\ell} = 0.0$ )

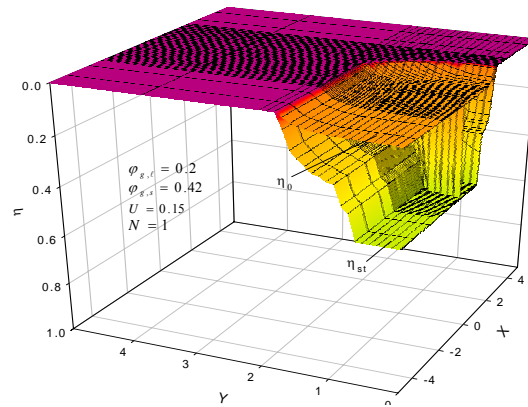


Fig. 6 Three-dimensional shape of the HAZ ( $\Delta_s = 0.25, U_b = 0.15, N = 1, \varphi_{g,\ell} = 0.2$ )

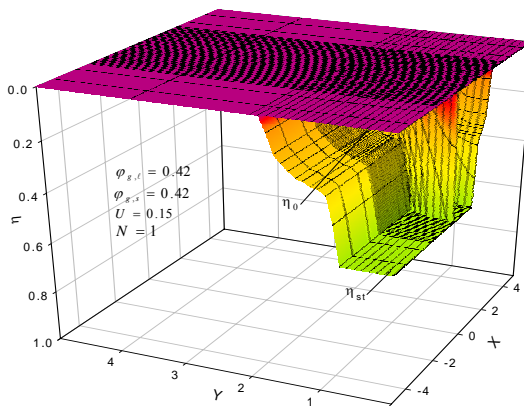


Fig. 7 Three-dimensional shape of the HAZ ( $\Delta_s = 0.25, U_b = 0.15, N = 1, \varphi_{g,\ell} = 0.42$ )

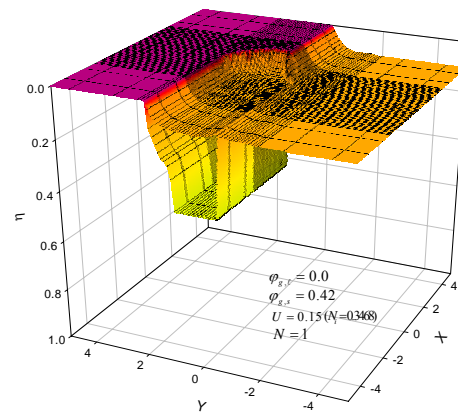


Fig. 8 Three-dimensional shape of the HAZ ( $\Delta_s = 0.25, U_b = 0.15, N = 1, \varphi_{g,\ell} = 0.0$ )

### Multiple-line scanning of loose powder on existing sintered layers

The optimum combinations of dimensionless laser beam intensity and scanning velocity are sought to obtain the expected sintering depth and the overlaps between the newly sintered layers and the existing sintered layers below. Before the frontier of the liquid pool reaches the expected sintering depth, the dimensionless laser beam intensity will increase by a little increment after the steady state is obtained for the given the dimensionless laser beam intensity and scanning velocity. The dimensionless laser beam intensity will not stop the increase until the required sintering depth and 50% overlap between HAZ and existing sintered layers underneath are obtained. The three dimensional shapes of the Heat Affected Zone (HAZ) with different  $\varphi_{g,\ell}$  with only one existing layer underneath for multiple laser scan lines are shown in Figs. 8-10. The scanning velocities are fixed at  $U_b = 0.15$  and the optimized laser intensity for each case is shown in the parenthesis in each figure. The shrinkage is smaller when the volume fraction of gas in the liquid pool increases and there is no shrinkage when  $\varphi_{g,\ell}$  is up to  $\varphi_{g,s}$ . The laser beam

intensity increases with increasing  $\varphi_{g,\ell}$  in order to obtain the same sintering depth and overlap since higher  $\varphi_{g,\ell}$  causes the smaller shrinkage and thicker existing sintered layers underneath. A part of the initially overlapped region which is the resolidified region after previous scanning re-melts again. Therefore, the neighbored scan lines can have a solid bond after the liquid metal resolidified again when the laser beam moves away.

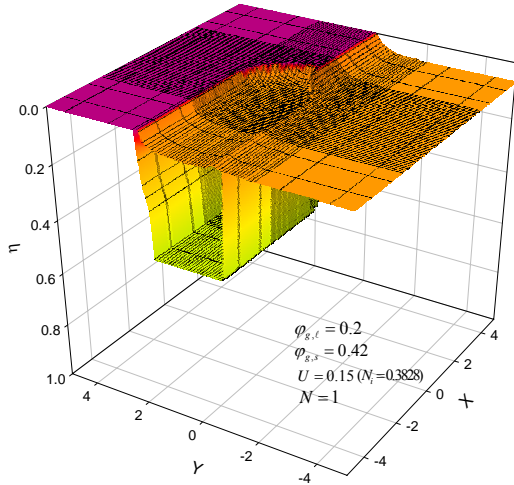


Fig. 9 Three-dimensional shape of the HAZ ( $\Delta_s = 0.25, U_b = 0.15, N = 1, \varphi_{g,\ell} = 0.2$ )

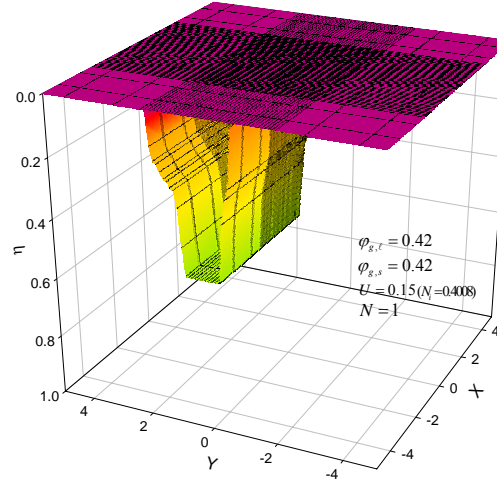


Fig. 10 Three-dimensional shape of the HAZ ( $\Delta_s = 0.25, U_b = 0.15, N = 1, \varphi_{g,\ell} = 0.42$ )

### Conclusions

Modeling of Direct Selective Laser Sintering of a two-component metal powder layer with the finite thickness is performed. The sintering process of a single loose powder layer and a loose powder layer on top of multiple existed sintered layers were investigated respectively. Overlaps between the newly sintered layer and pre-deposited sintered layers are considered in order to obtain the sound metallic bonding. The results indicate that the sintering depth and shape of HAZ significantly increases with increasing laser beam intensity and decreasing moving laser beam scanning velocity. The partial shrinkage model prescribes the varying volume fraction of the gas in HAZ which results in the different porosities between the powders and HAZ. The shrinkage will also be different due to the different porosity of HAZ.

### Acknowledgement

Support for this work by the Office of Naval Research under grant number N00014-04-1-0303 is gratefully acknowledged.

### Nomenclature

$Bi$	Biot number, $hR/k_H$
$Bo$	Bond Number, $\rho_\ell g R d_p / \gamma_m^0$
$C$	dimensionless heat capacity, $C^0 / C_H^0$
$C^0$	heat capacity, $\rho c_p$ , (J/m <sup>3</sup> -K)

$c_p$	specific heat, ( J/kg-K )
$d_p$	diameter of the powder particle ( m )
$g$	gravitational acceleration ( $m/s^2$ )
$h$	convective heat transfer coefficient, ( W/m <sup>2</sup> -K )
$h_{s\ell}$	latent heat of melting, J / kg
$\mathbf{i}$	unit vector in the x direction
$I_0$	laser intensity at the center of the laser beam, ( W/m <sup>2</sup> )
$\mathbf{j}$	unit vector in y direction
$k$	thermal conductivity, ( W/m-K )
$\mathbf{k}$	unit vector in z direction
$K$	permeability, or dimensionless thermal conductivity, $k/k_H$
$K_{r\ell}$	relative permeability
$Ma$	Marangoni number, $\gamma_m^0 d_p / (\alpha_H \mu)$
$N_i$	dimensionless laser intensity, $\alpha_a I_0 R / [k_H (T_m^0 - T_i^0)]$
$N_R$	radiation number, $\varepsilon_e \sigma (T_m^0 - T_i^0)^3 R / k_H$
$N_t$	temperature ratio for radiation, $T_m^0 / (T_m^0 - T_i^0)$
$p$	pressure ( N / m <sup>2</sup> )
$P_c$	dimensionless capillary pressure, $p_c / (\gamma_m^0 \sqrt{\varepsilon / K})$
$R$	radius of the laser beam at 1/e ( m )
$s$	solid-liquid interface location ( m )
$s_0$	location of surface ( m )
$s_{st}$	sintered depth ( m )
$Sc$	subcooling parameter, $C_L^0 (T_m^0 - T_i^0) / (\rho_L h_{s\ell})$
$T$	dimensionless temperature, $(T^0 - T_m^0) / (T_m^0 - T_i^0)$
$t$	false time ( s )
$T^0$	temperature ( K )
$u_b$	laser beam scanning velocity ( m / s )
$U_b$	dimensionless scanning velocity, $u_b R / \alpha_H$
$\mathbf{v}$	velocity vector, $u\mathbf{i} + v\mathbf{j} + w\mathbf{k}$
$\mathbf{V}$	dimensionless velocity vector, $\mathbf{v} R / \alpha_H$
$\forall$	volume ( m <sup>3</sup> )
$x, y, z$	coordinate, ( m )
$X, Y, Z$	dimensionless moving horizontal coordinate, $(x, y, z) / R$
<b>Greek symbol</b>	
$\alpha$	thermal diffusivity ( m <sup>2</sup> / s )
$\alpha_a$	absorbitivity
$\gamma^0$	surface tension, ( N / m <sup>2</sup> )
$\gamma_m^0$	surface tension of the low melting point metal at melting point, ( N / m <sup>2</sup> )

$\delta$	powder layer thickness, (m)
$\Delta$	dimensionless powder layer thickness, $\delta / R$
$\Delta T^0$	one-half of phase-change temperature range ( K )
$\Delta T$	one-half of dimensionless phase change temperature range
$\varepsilon$	porosity, $(\nabla_g + \nabla_\ell) / (\nabla_g + \nabla_\ell + \nabla_s + \nabla_H)$
$\varepsilon_e$	emissivity of surface
$\eta$	dimensionless location of the solid-liquid interface, $s / R$
$\eta_0$	dimensionless location of the surface, $s_0 / R$
$\eta_{st}$	dimensionless sintered depth, $s_{st} / R$
$\rho$	density ( $kg / m^3$ )
$\sigma$	Stefan-Boltzmann constant, $5.67 \times 10^{-8} W / (m^2 \cdot K^4)$
$\tau$	dimensionless false time, $\alpha_H t / R^2$
$\varphi$	volume fraction
$\dot{\Phi}_L$	dimensionless volume production rate of the liquid
$\psi$	saturation, $\varphi_\ell / \varepsilon$
$\nabla$	dimensionless gradient operator, $\mathbf{i}(\partial / \partial X) + \mathbf{j}(\partial / \partial Y) + \mathbf{k}(\partial / \partial Z)$

### Subscripts

$c$	capillary
$g$	gas(es)
$eff$	effective
$H$	high melting point powder
$i$	initial
$\ell$	liquid or sintered region
$L$	low melting point powder
$s$	solid (unsintered region)

### References

- [1] Conley, J. G., and Marcus, H. L., 1997, "Rapid prototyping and solid freeform fabrication," *Journal of Manufacturing Science and Engineering*, Vol. 119, pp. 811-816.
- [2] Karapatics, N., Egger, G., Gygax, P.E., and Glardon, R., 1999, "Optimization of Powder Layer Density in Selective Laser Sintering," *Procs. of Solid Freeform Fabrication Symposium 1999*, pp. 255-263.
- [3] Manzur, T., DeMaria, T., Chen, W., and Roychoudhuri, C., 1996, "Potential Role of High Powder Laser Diode in Manufacturing," presented at SPIE Photonics West Conference, San Jose, CA
- [4] Bunnell, D., 1995, *Fundamentals of Selective Laser Sintering of Metals*, Ph.D. Thesis, University of Texas at Austin.
- [5] Storch, S., Nellesen, D., Schaefer, G., and Reiter, R., 2003, "Selective Laser Sintering: Qualifying Analysis of Metal Based Powder Systems for Automotive Applications," *Rapid Prototyping Journal*, Vol. 9, pp. 240-251.
- [6] Simchi, A. and Pohl, H., 2003, "Effects of Laser Sintering Processing Parameters on the Microstructure and Densification of Iron Powder," *Materials Science and Engineering A*, V. 359, pp. 119-128.

- [7] Simchi, A., Petzoldt, F., and Pohl, H., 2003, "On the Development of Direct Metal Laser Sintering for Rapid Tooling," *Journal of Materials Processing Technology*, Vol. 141, pp. 319-328.
- [8] Lu, L., Fuh, J., and Wong, Y.-S., 2001, *Laser-induced Materials and Processes for Rapid prototyping*, Kluwer Academic Publishers, Boston, MA.
- [9] Taylor, C. M., Childs, T. H. C. C., 2001, "Thermal experiments in Direct Metal Laser Sintering," *Proceedings of Euro RP 2001*, Process Development Session.
- [10] Childs, T. H. C., Hauser, C., Tontowi, A. E., Taylor, C., 2000, "Simulation and Experimental Verification of Crystalline Polymer and Direct Metal Selective Laser Sintering," *Proceedings of the SFF Symposium 2000*, pp. 100-109.
- [11] Houser, C., Childs, T. H. C., Dalgarno, K. W., 1999, "Selective Laser Sintering of Stainless Steel 314 HC processed using room temperature powder beds," *Proceedings of the SFF Symposium 1999*, pp. 273-280.
- [12] Laoui, T., Wang, X., Childs, T. H. C., Kruth, J. P., and Froyen, L., 2000, "Laser Penetration in A Powder Bed During Selective Laser Sintering of Metal Powders: Simulations Versus Experiments," *Proceedings of the SFF Symposium 2000*, pp. 453-460.
- [13] Steinberger, J., Shen, J., Manetsberger, K., Muellers, J., 2000, "The Simulation of the SLS Process as the Basis of a Process Optimization," *Proceedings of the SFF Symposium 2000*, pp. 377-385.
- [14] Munjuluri, N., Agarwal, S., and Liou, F. W., 2000, "Process Modeling, Monitoring and Control of Laser Metal Forming," *Proceedings of the SFF Symposium 2000*, pp. 235-242.
- [15] Mughal, M., and Plumb, O. A., 1993, "Thermal Densification of Metal-Ceramic Composites," *Scripta Metallurgica et Materialia*, Vol. 29, pp. 383-388.
- [16] Zhang, Y. and Faghri, A., 1999, "Melting of a subcooled mixed powder bed with constant heat flux heating," *International Journal of Heat and Mass Transfer*, Vol 42, pp. 775-788.
- [17] Basu, B., and Srinivasan, J., 1988, "Numerical Study of Steady-State Laser Melting Problem," *International Journal of Heat Mass Transfer*, Vol. 31, No.11, pp. 2331-2338.
- [18] Zhang, Y., and Faghri, A., 1998, "Melting and Resolidification of a Subcooled Mixed Powder Bed with Moving Gaussian Heat Source," *ASME J. Heat Transfer* Vol. 120, pp. 883-891.
- [19] Raman R. and German R. M., 1995, "A Mathematical Model for Gravity-induced Distortion during Liquid-Phase Sintering," *Metallurgical and Materials Transactions A*, Vol. 26 A., pp. 653-659.
- [20] Kou. S., and Wang, Y. H., 1986, "Three-dimensional Convection in Laser Melted Pools," *Metallurgical and Materials Transactions A*, Vol. 17A, pp. 2265-2269.
- [21] Kolossov, S., Boillat, E., Glardon, R., Fisher, P., and Locher, M., 2004, "3D FE Simulation for Temperature Evolution in the Selective Laser Sintering Process," *International Journal of Machine Tools and Manufacture*, vol. 44, 117-123.
- [22] Zhang, Y., Faghri, A., Buckley, C. W., and Bergman, T. L., 2000, "Three-Dimensional Sintering of Two-Component Metal Powders with Stationary and Moving Laser Beams," *ASME J. Heat Transfer*, Vol. 122, pp. 150-158.
- [23] Pak, J., and Plumb, O. A., 1997, "Melting in a Two-Component Packed Bed," *J. Heat Transfer*, Vol. 119, pp. 553-559.
- [24] Cao, Y., and Faghri, A., 1990, "A Numerical Analysis of Phase Change Problems Including Natural Convection," *ASME J. Heat Transfer*, Vol. 112, pp 812-816.
- [25] Kaviany, M., 1995, *Principles of Heat Transfer in porous Media*, Springer-Verlag, New York.
- [26] Patankar, S. V., 1980, *Numerical Heat Transfer and Fluid Flow*, McGraw-Hill, New York.